A Global Climatology of Extratropical Transition

Part I: Characteristics Across Basins

Melanie Bieli*

Department of Applied Physics and Applied Mathematics, Columbia University, New York, NY

Suzana J. Camargo

Lamont-Doherty Earth Observatory, Columbia University, Palisades, NY

Adam H. Sobel

Department of Applied Physics and Applied Mathematics, Columbia University, New York, NY, and Lamont-Doherty Earth Observatory, Columbia University, Palisades, NY

Jenni L. Evans

Department of Meteorology and Atmospheric Science, Pennsylvania State University, University Park, PA

Timothy Hall

NASA Goddard Institute for Space Studies, New York, NY

Corresponding author address: Melanie Bieli, Department of Applied Physics and Applied Mathematics, Columbia University, New York, NY

E-mail: mb4036@columbia.edu

ABSTRACT

The authors present a global climatology of tropical cyclones (TCs) that undergo extratropical transition (ET). ET is objectively defined based on a TC's trajectory through the cyclone phase space (CPS), which is calculated using storm tracks from 1979-2015 best-track data and geopotential height fields from reanalysis datasets. Two reanalyses are used and compared for this purpose, the Japanese 55-year Reanalysis (JRA-55) and the ECMWF Interim Reanalysis (ERA-Interim). The results are used to study the seasonal and geographical distributions of storms undergoing ET and inter-basin differences in the statistics of ET occurrence.

About 50% of all storms in the North Atlantic and the Western North Pacific undergo ET. In the southern hemisphere, ET fractions range from about 20% in the South Indian Ocean and the Australian region to 40% in the South Pacific. The basins with the lowest ET fractions are the North Indian Ocean and the Central and Eastern North Pacific. In the North Atlantic and Western North Pacific, the probability of ET has a local minimum in the earlier part of the peak season and reaches the highest values prior to the peak season and toward its end. The seasonal cycles in the southern hemisphere are less pronounced. Landfalls by storms undergoing ET occur about 3 times per year in the North Atlantic and 7-10 times per year in the Western North Pacific, while coastal regions in the Australian region are affected once every 2-4 years.

1. Introduction

Toward the end of their lifetimes, tropical cyclones (TCs) often undergo a process called extratropical transition (ET), in which they change their physical structure and develop characteristics typical of extratropical cyclones. ET occurs as a TC moves into higher latitudes and encounters cooler sea surface temperatures and stronger vertical wind shear (Jones et al. 2003). The baroclinic environment sets the stage for the transition of the TC: As colder, drier air intrudes into the warm core, the storm loses its radial symmetry and begins to tilt toward the cold upper-level air. Eventually the TC becomes a cold-core system with asymmetric, frontal structure, completing its transition to an extratropical cyclone.

During ET, a storm may reintensify as it starts to tap baroclinic energy in addition to the energy source residing in the thermodynamic disequilibrium between the atmosphere and the underlying ocean. Often the system also accelerates its forward motion and produces intense precipitation, strong winds and large surface water waves, posing a serious threat to coastal regions and maritime activities (Jones et al. 2003). In particular, tropical systems that reintensify after ET in the North Atlantic can constitute a hazard for Canada and/or northwest Europe – e.g., the transitioning Hurricane Igor (2010) caused severe flooding in Newfoundland (Masson 2014), and the extratropical system that developed from Hurricane Lili (1996) was responsible for seven deaths and substantial economic losses in Europe (Agustí-Panareda et al. 2005). In October 2017, Hurricane Ophelia became the easternmost Atlantic major hurricane in recorded history and transformed into an extratropical cyclone that wreaked havoc on Ireland and Great Britain (Roseli et al. 2017).

However, not all TCs reintensify during ET – some decay, while others do not undergo transition at all, even when moving poleward into baroclinic regions. The extratropical fate of a TC is difficult to forecast – in general, the "rebirth" of a TC as an extratropical cyclone is more likely to

happen over ocean and when an upper-level trough approaching from the west connects with the tropical system (Emanuel 2005; Hart and Evans 2001; Matano and Sekioka 1971). This interaction may not only transform the storm, but also alter the large-scale midlatitude flow, causing poor synoptic predictability over a wide area downstream (e.g., Anwender et al. 2008; Keller 2012, 2017).

Around the turn of the millennium, the increasing awareness that the nature of a storm can change over the course of its life cycle sparked research on case studies of individual transitions (e.g., Atallah and Bosart 2003; McTaggart-Cowan et al. 2003; Thorncroft and Jones 2000) as well as on basin-specific climatologies (e.g., Foley and Hanstrum 1994; Hart and Evans 2001; Klein et al. 2000; Sinclair 2002). However, advances in research were hindered by the lack of an objective definition of ET. This gap was filled by the cyclone phase space (CPS) framework proposed by Hart (2003), which has since become well-established and widely used. Indeed, the development of the CPS was motivated by the study of ET; its effectiveness for this application was first demonstrated by Evans and Hart (2003).

The CPS allows for automated and objective detection of ET in large sets of storms and hence paved the way for statistical approaches to describe the phenomenon. This motivated more recent ET climatologies in various ocean basins (e.g., Kitabatake 2011; Wood and Ritchie 2014). However, these studies mostly focus on single ocean basins and use a variety of data sets. Moreover, they include different modifications to the original CPS-based definition of ET in Hart (2003), which makes their results difficult to compare.

This lack of a global perspective on ET has also recently been pointed out by Evans et al. (2017) and provides the motivation for the study at hand: Using a consistent set of data, time period, and method, we present a global CPS-based climatology of ET that encompasses all major cyclone basins. Following up on this study, Bieli et al. (2018; hereafter Part II) explore the CPS-based

definition of ET in further detail, by assessing its dependence on the underlying reanalysis dataset as well as its statistical performance in a comparison with the ETs defined by human forecasters.

2. Data and Methods

a. TC Best-Track and Reanalysis Datasets

The two basic ingredients for the analysis presented here are global TC track data and geopotential height fields from reanalysis datasets. Here we consider best-track datasets from the National Hurricane Center (NHC) in the North Atlantic (NAT) and in the Eastern and Central North Pacific (ENP), from the Joint Typhoon Warning Center (JTWC) in the North Indian Ocean (NI), the Southern Hemisphere (SH), and the Western North Pacific (WNP), and from the Japan Meteorological Agency (JMA) in the WNP. Within the SH, we distinguish the South Indian Ocean (SI), the Australian region (AUS), and the South Pacific (SP).

The best-track data provide information on the position of the storm center, maximum wind speed, and the type of the storm as declared by the respective operational meteorological agencies. In the best-track archives of the JTWC, the "storm type" records only start in 2003. For our analysis, we consider named TCs that occurred in the satellite era 1979-2015. Table 1 highlights the key characteristics of the resulting set of storms and complements Fig. 1, which shows a subset of the storm tracks examined in this study, together with the boundaries of the ocean basins.

In order to examine the sensitivity of the results with respect to the reanalysis dataset considered, all calculations were performed on the Japanese 55-year Reanalysis (JRA-55; $1.25^\circ \times 1.25^\circ$) released by the JMA (Kobayashi et al. 2015) as well as on the European Centre for Medium-Range Weather Forecasts' (ECMWF) Interim Reanalysis (ERA-Interim; $0.7^\circ \times 0.7^\circ$; Dee et al. 2011). Both datasets are considered state-of-the-art reanalyses and apply a four-dimensional vari-

ational data assimilation to provide dynamically consistent estimates of the state of the atmosphere in 6-hourly time steps. It is worth noting that the JRA-55 assimilation system uses artificial wind profile retrievals in the vicinity of TCs. Generated by synthetic dropwindsondes, they approximate the TC wind profile at the best-track locations and are then processed like observed data (Ebita et al. 2011; Hatsushika et al. 2006). ERA-Interim, on the other hand, does not assimilate any artificial TC information.

Schenkel and Hart (2012) found that there can be considerable position and intensity differences between the best-track TCs and the corresponding TCs in the reanalysis, especially for weak storms in observation-scarce regions. To gauge the effect of these possible mismatches, the best-track positions were mapped to the closest JRA-55 sea-level pressure minimum within a 300 km radius. However, the results derived from these recentered tracks barely differed from those of the original tracks and are therefore not included here.

b. Indices of Climate Variability

We use monthly sea surface temperature (SST) anomalies in the Niño 3.4 region (Barnston et al. 1997) provided by the Climate Prediction Center (CPC 2017) to define the phase of the El Niño Southern Oscillation (ENSO). In each basin, years with El Niño and La Niña conditions are defined according to the value of the Niño-3.4 index averaged over the months of its peak season (Table 1). If this value reaches a threshold of 0.5 (-0.5) and falls within a period of at least five consecutive overlapping three-month intervals exceeding that threshold, a year is considered an El Niño (La Niña) year. Thus, the ENSO phase of a given year may differ between basins with different peak seasons.

The Atlantic Meridional Mode (AMM) and Pacific Meridional Mode (PMM) SST indices developed by Chiang and Vimont (2004) are the result of a maximum covariance analysis of tropical

SSTs. Time series of monthly AMM and PMM indices are available from the NOAA Earth System Research Laboratory (NOAA ESRL 2017). The annual time series used to examine correlations with the occurrence of ET were obtained by taking the average over the peak season in each basin.

c. Cyclone Phase Space (CPS)

We employ the CPS proposed by Hart (2003) to objectively identify storms that undergo ET. In the CPS framework, the physical structure of cyclones is described based on three parameters that can all be computed from geopotential height fields: The B parameter measures the asymmetry in the geopotential thickness surrounding the cyclone, and two thermal wind (V_T) parameters assess whether the cyclone has a warm or cold core structure in the upper ($-V_T^U$) and lower ($-V_T^L$) troposphere (with the convention of the minus sign, positive values correspond to warm cores). In this study, we treat all three parameters as dimensionless quantities that have been normalized by their units.

The B parameter is computed by taking the difference between the average 900-600 hPa geopotential thickness to the right and to the left of the storm, in a radius of 500 km around the storm center:

$$B = h\left(\overline{Z_{600\text{ hPa}} - Z_{900\text{ hPa}}}\Big|_{\text{R}} - \overline{Z_{600\text{ hPa}} - Z_{900\text{ hPa}}}\Big|_{\text{L}}\right),$$

where Z is geopotential height, R indicates right relative to the storm motion, L indicates left relative to the storm motion, and the overbar indicates the areal mean over a semicircle of radius 500 km. The hemispheric parameter h is 1 for the northern hemisphere and -1 for the southern hemisphere. Thermally symmetric storms will thus have B values close to zero, while large B values represent thermally asymmetric storms.

The parameters $-V_T^L$ and $-V_T^U$ evaluate the thermal wind in the 900-600 hPa layer and the 600-300 hPa layer, respectively:

$$-V_T^L = \frac{\partial \Delta Z}{\partial (\ln p)}\bigg|_{900\text{ hPa}}^{600\text{ hPa}}$$

$$-V_T^U = \frac{\partial \Delta Z}{\partial (\ln p)}\bigg|_{600\text{ hPa}}^{300\text{ hPa}}$$

They are computed by linear regression of ΔZ, the difference in maximum and minimum geopotential height within 500 km of the storm's center, over seven pressure levels. The pressure levels range from 900 hPa to 600 hPa and from 600 hPa to 300 hPa, in increments of 50 hPa. Positive values of $-V_T^L$ and $-V_T^U$ (weakening geostrophic wind with height) then indicate the presence of a warm core in that layer, while strengthening winds with height lead to negative values and are associated with cold-cored systems.

TCs are characterized by small values of B and positive values of $-V_T^L$ and $-V_T^U$, while extratropical storms have large values of B and negative values of $-V_T^L$ and $-V_T^U$. As described by Hart (2003), transitioning storms typically follow a trajectory where the storm first loses its symmetry before developing a cold core in the lower troposphere. Evans and Hart (2003) then define the onset of ET as the time when the B parameter first exceeds a value of 10, while the drop of $-V_T^L$ below zero marks the end of the process. The two diagrams in Fig. 2 illustrate the idealized CPS trajectories of a storm undergoing ET, showing its evolution from a symmetric cyclone with a warm-core thermal structure to an asymmetric, cold-core cyclone.

For this study, no smoothing was applied to the CPS parameters, and building on the results of Part II, the original definition of ET has been modified with the purpose of maximizing the agreement with the ET cases in the best-track datasets: We increased the B threshold to 11 and required the cyclone to develop a cold-core structure throughout the 900-300 hPa layer for a successful ET completion, i.e., we required $-V_T^U$ (not just $-V_T^L$) to become negative. Evans and Hart (2003) argued that as the upper troposphere usually becomes cold prior to the lower troposphere, thermal

wind in the lower troposphere provides a more stringent criterion on transition completion than the upper-tropospheric thermal wind, and hence they did not impose any condition on $-V_T^U$. The inclusion of the $-V_T^U$ criterion is further discussed in section 3.b. In addition, ET onset was only declared if a storm had wind speeds of at least 33 kt, as some tropical depression-like systems or monsoonal troughs raise false alarms due to their asymmetric structure.

After computing the CPS parameters along all best-tracks (once in JRA-55 and once in ERA-Interim), we applied the CPS criteria to diagnose each TC either as an "ET storm" (i.e., a storm that undergoes ET at some point in its lifetime) or as a "non-ET storm" (i.e., a storm that does not undergo ET).

3. Results

a. CPS Parameters and Trajectories

The CPS parameters calculated along the TC tracks are the building blocks of this global ET climatology and provide the starting point of our analysis. Box plots of all six-hourly CPS parameters (Fig. 3) show that the medians of both thermal wind parameters are positive, indicating the dominant presence of warm-cored storms. The distributions of the B parameter are concentrated around zero, representing the fingerprint of thermally symmetric tropical storms. As we will show in section 3.b, the long tails extending into the extratropical parameter ranges in the NAT and the WNP (right tails for the B parameter, left tails for $-V_T^L$ and $-V_T^U$) will manifest themselves in high ET fractions in these two basins.

Due to the thresholds for asymmetry and cold-core structure, all CPS trajectories of transitioning storms exhibit some level of similarity. In general, though, individual trajectories of cyclones in the CPS are very diverse, demonstrating the wide range of possible structural evolutions the

storms can follow. Apart from the high degree of inter-storm variability, the CPS path for a given storm may also differ quite substantially depending on which dataset was used to calculate the CPS parameters. Fig. 4 illustrates this dependence using the example of Tropical Storm Earl (1992), whose trajectory in a B vs.$-V_T^L$ cross section of the CPS (Figs. 4a and 4b) looks markedly different for the two reanalyses used in this study. Earl does not undergo ET in JRA-55, while the ERA-Interim trajectory depicts a full transition to an extratropical system (for reference, Earl also becomes extratropical in the NHC best-track data).

On 06 UTC 3 October (the third-last track point), Earl is clearly visible in the relative vorticity fields at 850 hPa (Figs. 4c and 4d) of the two reanalyses, which feature a vortex centered northeast of Florida. The peak values are higher in ERA-Interim, but the differences in position and size of the storm in the two reanalyses are too small to explain the discrepancy in the CPS trajectories.

As expected from the B vs. $-V_T^L$ trajectory, the ΔZ profile (Fig. 4e) of JRA-55 decreases with height in the 900-600 hPa layer, indicating a warm core in the lower troposphere. This is consistent with the storm's position in the upper right "asymmetric warm-core" quadrant of the CPS. In contrast, the ERA-Interim profile shows increasing geostrophic wind (and thus a cold-core structure) throughout the 900-300 hPa layer – consequently, the storm is located in the upper left "extratropical" quadrant.

The following sections will make it clear that such differences between JRA-55 and ERA-Interim are not only visible in individually selected storms but also in the outcomes of climatological analyses.

b. Fraction

Fig. 5 juxtaposes the global ET fractions computed using the CPS and those obtained from the best-track labels. Note that the CPS-derived ET fractions in Fig. 5 refer to the time periods for

which best-track labels were available – in the case of the JTWC best-tracks, the available period is 2003-2015. An overview of all CPS-derived fractions for the entire time period 1979-2015 can be found in Table 2.

There are several notable differences among ocean basins as well as between the two reanalysis datasets: According to the JMA and NHC best-track data, 48% of the storms in the WNP and 45% of the storms in the NAT undergo ET. Compared to these two basins, ET is very rare in the ENP and the NI (2.8% and 1.5%, respectively). The low ET fraction in the ENP is mostly the result of a strong subtropical ridge over southwestern North America, which exerts its influence over much of the hurricane season and tends to steer the cyclones westward away from land, keeping them in low latitudes (Wood and Ritchie 2014). In the NI, northward moving storms usually make landfall before reaching a sufficiently baroclinic environment to undergo transition. Of the SH basins, the SP (44%) has a considerably higher ratio of ET storms than the SI (27%) and the AUS (20%).

With the exceptions of the SP and the SI, the ERA-Interim fractions exceed the JRA-55 values and the observations, particularly in the ENP and the NI. This pattern is robust even when considering the sensitivity to various definitions of ET onset and ET completion, e.g., when varying the $-V_T^L$ and $-V_T^U$ thresholds from 0 to -10. A two-sample, two-sided t-test confirms the statistical significance of the differences between the ET fractions of the two reanalyses for each basin. The t-test was performed using sample means and sample standard deviations obtained from repeatedly ($n = 1000$) computing the ET fractions on randomly sampled subsets (5 years) of storms.

ET fractions depend not only on the basin and the reanalysis dataset, but also on the best-track archive: In the WNP, the percentage of storms undergoing ET in the JMA dataset exceeds that in the JTWC dataset by 6.4 percentage points (Fig. 5). This discrepancy is even more pronounced in the objective, CPS-based ET fractions, indicating that its primary reason lies in the tracks themselves rather than in different operational practices at the warning centers. Indeed, Fig. 6 reveals

that the JMA best-tracks extend farther northeast: Their average end position is 32°N, 141°E (standard deviation: 14°, 28°), while the average JTWC best-track ends at 28°N, 131°E (standard deviation: 10°, 22°). Thus, the JMA storms veer more frequently into the midlatitude zone where ET tends to occur. Of all cyclones that undergo ET along the JMA best-track but not along the JTWC best-track, about 80% complete ET farther north than the latitude of the last JTWC track point. Given that the JMA labels are available over a longer time period and that the JMA best-tracks have a better performance than the JTWC best-tracks (as shown in Part II), all results for the WNP presented in the rest of this study are based on the JMA archive.

Past studies on ET climatologies have mostly focused on single ocean basins and differ considerably in their methods (e.g., some of them apply objective techniques such as the CPS while others use warning center labels or satellite images), as shown in the papers summarized in Table 3. The large difference between the estimates for the WNP obtained by Klein et al. (2000) and Kitabatake (2011) illustrates the dependence of the ET climatology on the methodology, dataset, time period, and sample size. Another example of this dependence is the study by Studholme et al. (2015), who analyzed northern hemisphere TCs tracked in ERA-Interim. Using a combination of CPS and a k-means clustering, they accounted for multiple pathways of ET. This approach resulted in ET fractions that are higher than the values of other climatologies (including the one presented here), and Studholme et al. (2015) speculate that this might be a consequence of their longer tracks, which allow more time for ET to occur.

Our ET percentage of 46.7% for the WNP obtained from JRA-55 is comparable to the value of 40% in Kitabatake (2011), who used the JRA-25 reanalysis. Tracking North Atlantic storms in ERA-Interim, Zarzycki et al. (2016) computed an ET fraction of 55.2%, which agrees with the fraction of 53.7% yielded by our ET detection in the NAT best-track storms in ERA-Interim.

According to Wood and Ritchie (2014), 9% of the storms in the ENP undergo ET, which is about twice the 4.8% we obtain using the same dataset and a similar time period. This difference is mainly a consequence of the fact that Wood and Ritchie (2014) used a definition of ET which did not require $-V_T^U$ to cross any threshold. Indeed, if we remove the condition on $-V_T^U$, the calculated ET fraction in the ENP rises to 8.0%. Thus, a lower-tropospheric cold core is not necessarily preceded by the development of a cold core in the upper troposphere – in other words, the requirement for an upper-tropospheric cold-core for ET completion is not a redundant criterion. In fact, with the notable exception of the NAT, the effect of ignoring the $-V_T^U$ parameter in the definition of ET completion is even larger in other ocean basins, especially for ERA-Interim. The original CPS framework presented in Hart (2003) had been tailored to the NAT, and in that basin, the ET rates are not sensitive to the upper-tropospheric parameter. However, considering that there is no absolute truth in the definitions of ET onset and completion, the requirement on the upper-tropospheric thermal structure in the definition of ET completion has been added in this study because it clearly improves the agreement with the best-tracks on a global basis, as shown in greater detail in Part II.

c. Seasonal Cycle

There is substantial variability in the seasonal patterns of ET events in the different basins (Fig. 7). However, as there is a good agreement between the two reanalyses, Fig. 7 only shows the results for JRA-55. In the NAT, the number of ET storms is highest in September, but the ET fraction only reaches its peak in November. A similar seasonal cycle was obtained by Hart and Evans (2001) based on the storm type labels in the NHC best-tracks. The observed increase in ET fraction from summer to fall is explained by the combined effect of the delayed warming of the ocean and seasonal changes in the equatorward extent of the region that is conducive to growth of

baroclinic instabilities (e.g., Hart and Evans 2001): In summer, a TC leaving the area that supports tropical development often can't reach a baroclinically favorable region before weakening too much for a transition to occur. In later months, however, this gap closes because the baroclinically favorable region pushes southward and encroaches on the area over which tropical development can occur – due to the large heat capacity of the ocean, this "tropically favorable" region still extends relatively far north at that time of the year. Thus, the environment is most ET-friendly in October and November, which is consistent with the increased transition probability in these months. A seasonal climatology of vertical wind shear between 200 hPa and 850 hPa (Fig. 8) confirms that the peak season in the NAT takes place in an environment of weak baroclinicity, which grows stronger toward the end of the hurricane season.

The WNP shows a double peak in May and September, which is consistent with the result of Kitabatake (2011). In contrast to the other basins, the WNP has TCs forming all year round, but the months that overlap with the NAT hurricane season (June - November) show a similar drop of the ET percentage in summer, followed by higher values in fall. However, while the transition probability in the WNP decreases after September, it continues to rise in the NAT until the end of the season. The decrease of the ET fraction in the WNP in late fall coincides with the development of a zone of high vertical wind shear (Fig. 8), which restricts the formation of TCs to the Pacific warm pool and low latitudes (Camargo et al. 2007). TCs originating in these regions often move in straight westward tracks, whereas storms that recurve (and are more likely to undergo ET) tend to form farther north (Camargo et al. 2007) and are thus underrepresented during that time of the year. In May, TCs in the WNP have the highest ET probability of all months. In order to have such an overall ET peak in May despite the relative scarcity of recurving tracks in that month (Camargo et al. 2007), the ET probability of those few storms that do recurve must be high – this was also noted by Kitabatake (2011).

The SH basins exhibit much less pronounced seasonal cycles of ET than the NAT or the WNP. In the SH, the extension of the subtropical jet into tropical latitudes acts to constrain the tracks of TCs to lower latitudes than in the northern hemisphere (Krishnamurti et al. 2013). In addition, the seasonal change of the baroclinic energy source is relatively small except near the Antarctic (Zhu 2003). Thus, throughout the year, TCs in the SH encounter a fairly strong baroclinic environment already at low latitudes, which is also illustrated in Fig. 8. Compared to the other basins, the NI and the ENP have very low ET rates and do not show a clear seasonality.

d. Interannual Variability

Time series of ET fractions (Fig. 9) reveal the interannual variability in the percentages of storms undergoing ET. The magnitudes of the year-to-year fluctuations in each basin reflect the variances in the distributions of the annual ET counts, which are driven by variances in the fraction of TCs that transition and the annual TC counts. For example, the variability in the NI is dominated by the combination of a low ET fraction and a low overall storm count. Except for the JRA-55 time series in the SI, the slopes of the linear regression lines are not statistically significant at the 95% confidence level (Table 4). Fig. 9 also makes it clear that the higher overall ET fractions associated with the CPS parameters calculated in ERA-Interim (Fig. 5 and Table 2) are present in nearly all individual years.

Analyses in each basin of the best-track time series of ET fractions using a Poisson model of constant annual-mean TC formation and a constant probability per TC of undergoing ET suggest that the interannual variability is largely consistent with a stationary random process in the NAT, WNP, AUS, and the SI (not shown). Also, there is no significant lag-one autocorrelation in any of these time series (not shown), indicating the absence of year-to-year memory in the transition

probability. Due to low ET and/or total TC counts, autocorrelation and consistency with a Poisson process were not evaluated for the ENP, NI, or SP.

The correlations between the time series of JRA-55 and ERA-Interim (Table 4) are high and statistically significant for the NAT and the WNP. In the three SH basins and the NI, the correlations between the ET fractions in the two reanalyses are also statistically significant, but weaker. The ENP is the only basin where the correlation between the two reanalyses is not significant.

e. Spatial Patterns

Defining the track density as the sum of all best-track data points located in each $1.25^\circ \times 1.25^\circ$ box of the latitude/longitude grid used in JRA-55, Fig. 10 compares the spatial distributions of ET storms with those of non-ET storms, using the JRA-55 classification. Track densities from ERA-Interim (not shown) qualitatively agree with those from JRA-55. To first order, TCs are steered by the predominant large-scale circulation: After their formation in the tropics, they generally track westward in the easterly flow on the equatorward side of a subtropical ridge. Then, moving around the periphery of the anticyclone, they drift poleward until they possibly recurve with the midlatitude westerlies. This general track pattern holds in all basins except in the SP, where a majority of the storms move in a southeasterly direction (e.g., Ramsay et al. 2012).

Due to the scarcity of ET events in the NI and the ENP, this part of the analysis focuses on the NAT, the WNP, and the SH. In the NAT and the WNP, ET storms recurve to a greater extent than the non-ET storms, which typically follow an east-west path with less poleward drift. As a result of this recurvature, the highest density of ET storms in the WNP is found in the East China Sea, while the concentration of non-ET storms peaks farther southwest, in the South China and Philippine Seas. Although the track density in the NAT is more homogeneously distributed throughout the basin than in the WNP, the general pattern is similar: ET storms most frequently

pass the area off the coast of the southeast United States, and non-ET storms have their highest density southwest of that area, in the Gulf of Mexico (Fig. 10).

Most SH storms that undergo ET occur northeast of Australia, mainly in the SP. This is a region where the density of non-ET storms is rather low compared to the SI and the western part of the AUS. Thus, the storms passing that area have a high probability of transition. Indeed, as shown in Fig. 5, the ET fraction in the SP is about 40%, considerably higher than in the SI and the AUS, where on average only about every fifth storm undergoes ET. At its peak in March, the ET fraction in the SP exceeds 60% (Fig. 7). Composites of vertical wind shear for the peak months of the SH season (Fig. 11) show that this peak occurs in the presence of a strong baroclinic forcing.

The genesis locations of ET storms and non-ET storms (not shown) are fairly similar. In particular, there is no strongly localized "hot spot" of ET storm formation in any northern hemisphere basin – in fact, the genesis positions of ET storms in the NAT and the WNP are overall more homogeneously distributed than those of their non-ET counterparts. However, this relatively even spread of genesis locations in the cumulative view does not preclude the existence of seasonal variations (e.g., such as those found in the NAT by Hart and Evans 2001). The SH ET storms predominantly form in the SP, which is the region where we also find the highest track density of ET storms.

Statistics of the latitudes where TCs complete their transitions into extratropical cyclones are given in Fig. 12. As a reminder, the criterion for ET completion in this study is the development of a cold-core structure throughout the 900-300 hPa layer. The median latitude of ET completion in the seven basins ranges from about 20° to 40°, and these inter-basin variations are substantially greater than the differences between the two reanalyses.

In the NAT and the WNP, ET completion takes place substantially farther poleward than in the other basins. Furthermore, the decomposition into monthly statistics reveals the presence of a

distinct annual cycle in the ET latitude in both basins: Transition occurs at higher latitudes during the peak of the season and shifts to lower latitudes during the early and later months. In the NAT, these seasonal patterns of ET latitude are negatively correlated with those of the ET fractions (Fig. 7), i.e., months with high ET rates (e.g., November) have lower latitudes of ET completion, and vice versa. The correlation is not as strong in the WNP, where the decreasing ET latitudes in October-December are not associated with an increase in ET fraction. This is consistent with the idea that the WNP is dominated by straight-moving storms at that time of the year.

The SH ETs occur at lower latitudes than in the NAT and the WNP and do not have a distinct seasonal pattern. These features are consistent with the narrower latitudinal extent of the TC tracks in the SH, which reduces the exposure to the seasonal effects of advancing and retreating regions of baroclinic activity. The median latitudes of ET completion in the ENP and the NI are similar to those of the SH basins, but due to the scarcity of ET in these basins Fig. 12 does not show their monthly statistics.

f. Landfall

TC damage largely depends on landfalling storms, and some of these storms undergo ET before, while, or after they hit the coast. Table 5 provides a summary of the landfall events recorded in the best-track data, dividing the storms into tropical storms, transitioning storms, and extratropical storms (i.e., storms that have completed ET). Note that this classification refers to the nature of a storm at the time when the landfall occurs and does not make any statement on its further structural evolution – e.g., a TC that does not show any signs of a transition when reaching land might still undergo ET at a later stage despite falling into the "tropical" category in Table 5. If a single TC makes multiple landfalls, we count each individual landfall.

As a result of the geometry of the basins and the predominant large-scale circulation, the landfall ratios span a large range: At the extreme ends, almost three out of four storms in the NI move over land at least once in their lifetimes, but only about one out of seven in the ENP and the SP. In all basins, storms with tropical characteristics account for a clear majority of all landfall events, and more landfalling storms are of tropical nature in JRA-55 than in ERA-Interim. The NAT, WNP, and the SP, which have the highest overall ET fractions, also have the highest fractions of landfalls by transitioning or extratropical systems.

There is a discrepancy between JRA-55 and ERA-Interim in the ENP: According to the JRA-55-based CPS parameters, more than 90% of all landfalling storms are symmetric and warm-cored, while ERA-Interim classifies a fourth of them as extratropical. This suggests that ERA-Interim's higher overall ET fraction (Fig. 5) is the result of TCs that undergo ET over the ocean, rather than a consequence of structural changes in the wake of landfalls that might push storms into the asymmetric region of the CPS or increase the average position difference between the storm center in the best-tracks and in the reanalysis. It is notable that in terms of absolute numbers, the difference in the WNP – 249 landfalls by transitioning or extratropical storms in JRA-55, compared to 352 in ERA-Interim – is even higher than that in the ENP.

Fig. 13 shows the tracks of all TCs that make landfall as a transitioning or extratropical system at least once in their lifetimes. The locations of ET completion in the WNP are clustered in a region between about 25°N and 45°N centered over Japan, whereas completion in the NAT happens preferentially along the east coast of the United States and Canada. In both basins, the tracks in Fig. 13 represent about 80% of the total landfalling storms that undergo ET at some point in their lives – i.e., approximately 20% of the landfalling storms that undergo ET only begin to transition after landfall. When staying over land, such "post-landfall transitioners" can still cause substantial damage during and after their transition (e.g., Sousounis and Desflots 2010).

Of all basins, coastal regions in the NAT and the WNP are most frequently affected by transitioning or extratropical storms. During the 1979-2015 period, such landfall events happen about three times per year in the NAT, and 7-10 times per year in the WNP. In the SH, landfalling ET storms mainly pose a threat within the AUS region, especially Western Australia and the islands in the Coral and Tasman Seas. However, with a frequency of about one ET landfall every 2-4 years, the rate is substantially lower than in the NAT or the WNP.

g. Transition Time Periods

Defining the transition period as the time between the onset ($B > 11$) and the completion ($-V_T^U < 0$ and $-V_T^L < 0$) of ET, we find that in most basins, the average ET takes between one and two days. Table 6 lists all transition periods together with the p-value of a two-sided t-test on the sample means of the two reanalyses in each basin. However, comparing the transition periods between individual basins is not possible due to the large inter-reanalysis differences – e.g., in the WNP, the CPS parameters from ERA-Interim yield a mean transition period of 56 h, which is one day longer than the average ET duration in JRA-55. With the exception of the NAT, the transition periods in ERA-Interim are longer than those of JRA-55 in all other basins as well.

Evans and Hart (2003) obtained a mean transition period of about 33 h for the NAT, which agrees well with the 35 h (38 h) from ERA-Interim (JRA-55). On the other hand, our results for the WNP clearly exceed the average ET duration of about 17 h found by Kitabatake (2011).

There is an important caveat to be aware of in this examination of transition periods: For TCs that undergo ET by first developing a cold-core structure before becoming asymmetric, the ET onset coincides with the ET completion, resulting in a transition period of 0 h. This issue was also noted by Kitabatake (2011). The statistics in Table 6 include all these cases – when they are removed, the mean transition period in each basin typically increases by about 10-20 h.

h. Relationship with ENSO, AMM, and PMM

Natural climate variability strongly modulates the seasonal statistics of TCs. In most basins, ENSO is the primary driver of variability (Frank and Young 2007). In particular, ENSO exerts a well-defined control on TC occurrence and tracks in the WNP and the NAT (e.g., Wang and Chan 2002; Camargo and Sobel 2005; Bell and Chelliah 2006). Atlantic TC activity is also influenced by the Atlantic meridional mode (AMM), which is associated with shifts in the cyclone genesis regions on interannual-to-decadal timescales (Vimont and Kossin 2007). Similarly, the Pacific meridional mode (PMM) has been associated with changes in TC activity in the WNP, with the positive PMM phase favoring the genesis of TCs and the negative PMM phase inhibiting their occurrence (Zhang et al. 2016).

Using the JRA-55 classification, correlating time series of ET fractions with the Nino3.4 index does not reveal a statistically significant linear relationship in any basin (Table 7), and no statistically significant relations are found for the PMM index either. Rather unexpectedly, the AMM index is significantly correlated with the ET fraction in the AUS and the SP. In contrast, the known connections between the AMM and TC activity in the NAT (e.g., Kossin et al. 2010; Vimont and Kossin 2007), the WNP (Zhang et al. 2017), and the ENP (Patricola et al. 2017) do not manifest themselves in significant correlations with the ET fractions. This suggests that the AMM influences these basins in ways whose net effect leaves the ET fraction unchanged, e.g., by changing the number of TCs rather than their tracks. The corresponding results using the ERA-Interim classification (not shown) only differ in the WNP, where the enhancement of the ET fraction during El Niño years is statistically significant. In particular, the correlation of the AMM index with the ET fraction in the AUS and the SP is robust with respect to the reanalysis considered. However, without a plausible physical mechanism, such a signal requires further corroboration.

For the NAT and the WNP, Fig. 14 shows the difference between the track density of ET storms occurring during the peak season of El Niño years and those forming during the peak season of La Niña years, normalized by the number of El Niño and La Niña years, respectively. In the WNP, cyclones in El Niño years have a stronger tendency to recurve northeastward and reach latitudes farther north (Wang and Chan 2002). Also, the mean cyclone genesis region is displaced to the southeast during El Niño years (Wang and Chan 2002; Chia and Ropelewski 2002). These two associations are consistent with Fig. 14: During El Niño years, more storms reach high latitudes, and more storms form in the easternmost genesis region. However, the positive correlation between the fraction of storms undergoing ET and the Nino3.4 index (Table 7) is not statistically significant. In the NAT, the difference in the tracks of ET storms between El Niño and La Niña years shows a less systematic pattern.

4. Summary and Concluding Remarks

This paper presents a global climatology of tropical cyclones (TCs) that undergo extratropical transition (ET) in the time period 1979-2015. The climatology is based on objective ET detection in the cyclone phase space (CPS), calculated from JRA-55 and ERA-Interim reanalysis data.

Our findings can be summarized as follows:

- ET fractions vary substantially between the seven basins examined here: At the top end, about half of the storms in the North Atlantic (NAT) and the Western North Pacific (WNP) undergo ET, followed by a transition rate of about 40% in the South Pacific (SP). ET occurs less frequently in the South Indian Ocean (SI) and the Australian region (AUS), where approximately every fifth storm transitions, and only in rare cases in the Eastern and Central North Pacific (ENP) and the North Indian Ocean (NI). In the NI, continental landmass stands in the way

of northward moving storms, while a strong subtropical ridge over southwest North America generates a westward steering flow that prevents ET from occurring in the ENP.

- There are differences in the seasonal cycles of ET in the NAT, the WNP, and the SH basins: The ET fraction maximizes later in the NAT than in the WNP, but both basins exhibit a local minimum in the earlier part of the peak season. We suggest that the interplay of tropical and baroclinic regulation, which is thought to be responsible for the November peak in the NAT, might be a weaker determinant of the transition probability for the fall season in the WNP due to the prevalence of straight westward-moving storms at that time of the year. In the SH basins, the ET fractions vary much less throughout the season, which is conceivably related to the narrower meridional confinement of the tracks.

- Of all basins, coastal regions in the NAT and the WNP are most frequently affected by TCs that have started or completed ET. During the 1979-2015 period, such landfall events happen about three times per year in the NAT, 7-10 times per year in the WNP, and once every 2-4 years in the AUS region.

- With the exception of the SI, time series of annual ET fractions from 1979 to 2015 do not show any statistically significant trends at the 95% confidence level.

- The choice of the reanalysis dataset used to calculate the CPS parameters has a substantial impact on the resulting climatology. Most notably, ET fractions derived in ERA-Interim in most cases exceed those calculated in JRA-55 (and often also the ET observations archived in the best-tracks), especially in the ENP. In Part II, we examine these differences in more detail, by comparing the CPS-based identification of ET storms in JRA-55 and ERA-Interim to the ET storms defined in the best-track datasets by human forecasters.

Acknowledgments. The authors would like to thank Dr. Robert Hart for providing Grid Analysis and Display System (GrADS) scripts that facilitated the development of the Python code used in this study. The funding for this research was provided by NASA under grant NNX15AJ05A, and by NSF under grant ATM-1322532.

References

Agustí-Panareda, A., S. L. Gray, G. C. Craig, and C. Thorncroft, 2005: The extratropical transition of tropical cyclone Lili (1996) and its crucial contribution to a moderate extratropical development. *Mon. Wea. Rev.*, **133 (6)**, 1562–1573, doi:10.1175/MWR2935.1.

Anwender, D., P. A. Harr, and S. C. Jones, 2008: Predictability associated with the downstream impacts of the extratropical transition of tropical cyclones: Case studies. *Mon. Wea. Rev.*, **136 (9)**, 3226–3247, doi:10.1175/2008MWR2249.1.

Atallah, E. H., and L. F. Bosart, 2003: The extratropical transition and precipitation distribution of hurricane Floyd (1999). *Mon. Wea. Rev.*, **131 (6)**, 1063–1081, doi:10.1175/1520-0493(2003)131⟨1063:TETAPD⟩2.0.CO;2.

Barnston, A. G., M. Chelliah, and S. B. Goldenberg, 1997: Documentation of a highly ENSO-related SST region in the equatorial Pacific: Research note. *Atmos.–Ocean*, **35 (3)**, 367–383.

Bell, G. D., and M. Chelliah, 2006: Leading tropical modes associated with interannual and multidecadal fluctuations in North Atlantic hurricane activity. *J. Climate*, **19 (4)**, 590–612, doi:10.1175/JCLI3659.1.

Bieli, M., S. J. Camargo, A. H. Sobel, J. L. Evans, and T. Hall, 2018: A global climatology of extratropical transition. Part II: Statistical performance of the cyclone phase space. *J. Climate*.

Camargo, S. J., A. W. Robertson, S. J. Gaffney, P. Smyth, and M. Ghil, 2007: Cluster analysis of typhoon tracks. Part I: General properties. *J. Climate*, **20 (14)**, 3635–3653, doi:0.1175/JCLI4188.1.

Camargo, S. J., and A. H. Sobel, 2005: Western North Pacific tropical cyclone intensity and ENSO. *J. Climate*, **18 (15)**, 2996–3006.

Chia, H. H., and C. Ropelewski, 2002: The interannual variability in the genesis location of tropical cyclones in the northwest Pacific. *J. Climate*, **15 (20)**, 2934–2944, doi:10.1175/1520-0442(2002)015⟨2934:TIVITG⟩2.0.CO;2.

Chiang, J., and D. Vimont, 2004: Analogous meridional modes of atmosphere–ocean variability in the tropical Pacific and tropical Atlantic. *J. Climate*, **17 (21)**, 4143–4158, doi:10.1175/JCLI4953.1.

CPC, 2017: Climate Prediction Center - Monitoring & Data: Current Monthly Atmospheric and Sea Surface Temperatures Index Values. URL http://www.cpc.ncep.noaa.gov/data/indices/.

Dee, D. P., and Coauthors, 2011: The ERA-Interim reanalysis: Configuration and performance of the data assimilation system. *Quart. J. Roy. Meteor. Soc.*, **137 (656)**, 553–597, doi:10.1002/qj.828.

Ebita, A., and Coauthors, 2011: The Japanese 55-year Reanalysis "JRA-55": An interim report. *SOLA*, **7**, 149–152, doi:10.2151/sola.2011-038.

Emanuel, K., 2005: *Divine wind: The history and science of hurricanes*. Oxford University Press.

Evans, C., and Coauthors, 2017: The extratropical transition of tropical cyclones. Part I: Cyclone evolution and direct impacts. *Mon. Wea. Rev.*, **145 (11)**, 4317–4344, doi:10.1175/MWR-D-17-0027.1.

559 Evans, J. L., and R. E. Hart, 2003: Objective indicators of the life cycle evolution of ex-
560 tratropical transition for Atlantic tropical cyclones. *Mon. Wea. Rev.*, **131 (5)**, 909–925, doi:
561 10.1175/1520-0493(2003)131⟨0909:OIOTLC⟩2.0CO;2.

562 Foley, G. R., and B. N. Hanstrum, 1994: The capture of tropical cyclones by cold fronts off
563 the west coast of Australia. *Wea. Forecasting*, **9 (4)**, 577–592, doi:10.1175/1520-0434(1994)
564 009⟨0577:TCOTCB⟩2.0.CO;2.

565 Frank, W. M., and G. S. Young, 2007: The interannual variability of tropical cyclones. *Mon. Wea.*
566 *Rev.*, **135 (10)**, 3587–3598, doi:10.1175/MWR3435.1.

567 Griffin, K. S., and L. F. Bosart, 2014: The extratropical transition of tropical cyclone Edisoana
568 (1990). *Mon. Wea. Rev.*, **142 (8)**, 2772–2793, doi:10.1175/MWR-D-13-00282.1.

569 Hart, R. E., 2003: A cyclone phase space derived from thermal wind and thermal asymmetry. *Mon.*
570 *Wea. Rev.*, **131 (4)**, 585–616, doi:10.1175/1520-0493(2003)131⟨0585:ACPSDF⟩2.0.CO;2.

571 Hart, R. E., and J. L. Evans, 2001: A climatology of the extratropical transition of Atlantic tropical
572 cyclones. *J. Climate*, **14 (4)**, 546–564, doi:10.1175/1520-0442(2001)014⟨0546:ACOTET⟩2.0.
573 CO;2.

574 Hatsushika, H., J. Tsutsui, M. Fiorino, and K. Onogi, 2006: Impact of wind profile retrievals on
575 the analysis of tropical cyclones in the JRA-25 reanalysis. *J. Meteor. Soc. Japan. Ser. II*, **84 (5)**,
576 891–905, doi:10.2151/jmsj.84.891.

577 Jones, S. C., and Coauthors, 2003: The extratropical transition of tropical cyclones: Forecast
578 challenges, current understanding, and future directions. *Wea. Forecasting*, **18 (6)**, 1052–1092,
579 doi:10.1175/1520-0434(2003)018⟨1052:TETOTC⟩2.0.CO;2.

Keller, J. H., 2012: *Diagnosing the downstream impact of extratropical transition using multi-model operational ensemble prediction systems*, Vol. 57. KIT Scientific Publishing.

Keller, J. H., 2017: Amplification of the downstream wave train during extratropical transition: Sensitivity studies. *Mon. Wea. Rev.*, **145 (4)**, 1529–1548, doi:10.1175/MWR-D-16-0193.1.

Kitabatake, N., 2011: Climatology of extratropical transition of tropical cyclones in the western North Pacific defined by using cyclone phase space. *J. Meteor. Soc. Japan. Ser. II*, **89 (4)**, 309–325, doi:10.2151/jmsj.2011-402.

Klein, P. M., P. A. Harr, and R. L. Elsberry, 2000: Extratropical transition of western North Pacific tropical cyclones: An overview and conceptual model of the transformation stage. *Wea. Forecasting*, **15 (4)**, 373–395, doi:10.1175/1520-0434(2000)015⟨0373:ETOWNP⟩2.0.CO;2.

Kobayashi, S., and Coauthors, 2015: The JRA-55 reanalysis: General specifications and basic characteristics. *J. Meteor. Soc. Japan. Ser. II*, **93 (1)**, 5–48, doi:10.2151/jmsj.2015-001.

Kossin, J. P., S. J. Camargo, and M. Sitkowski, 2010: Climate modulation of North Atlantic hurricane tracks. *J. Climate*, **23 (11)**, 3057–3076, doi:10.1175/2010JCLI3497.1.

Krishnamurti, T., L. Stefanova, and V. Misra, 2013: *Tropical Meteorology*. Springer Atmospheric Sciences, Springer New York, New York, NY, dOI: 10.1007/978-1-4614-7409-8.

Masson, A., 2014: The extratropical transition of hurricane Igor and the impacts on Newfoundland. *Natural hazards*, **72 (2)**, 617–632, doi:10.1007/s11069-013-1027-x.

Matano, H., and M. Sekioka, 1971: Some aspects of extratropical transformation of a tropical cyclone. *J. Meteor. Soc. Japan. Ser. II*, **49**, 736–743.

McTaggart-Cowan, R., J. R. Gyakum, and M. K. Yau, 2003: The influence of the downstream state on extratropical transition: Hurricane Earl (1998) case study. *Mon. Wea. Rev.*, **131 (8)**, 1910 – 1929, doi:10.1175//2589.1.

NOAA ESRL, 2017: Climate Timeseries. URL https://www.esrl.noaa.gov/psd/data/timeseries/monthly/.

Patricola, C. M., R. Saravanan, and P. Chang, 2017: A teleconnection between Atlantic sea surface temperature and eastern and central North Pacific tropical cyclones. *Geophys. Res. Lett.*, **44 (2)**, 1167–1174, doi:10.1002/2016GL071965.

Ramsay, H. A., S. J. Camargo, and D. Kim, 2012: Cluster analysis of tropical cyclone tracks in the Southern Hemisphere. *Climate Dyn.*, **39 (3)**, 897–917, doi:10.1007/s00382-011-1225-8.

Roseli, H., J. Prieto, I. Smiljanic, S. Lancaster, and J. Asmus, 2017: Hurricane Ophelia's transition – EUMETSAT. URL https://www.eumetsat.int/website/home/Images/ImageLibrary/DAT_3678625.html.

Schenkel, B. A., and R. E. Hart, 2012: An examination of tropical cyclone position, intensity, and intensity life cycle within atmospheric reanalysis datasets. *J. Climate*, **25 (10)**, 3453–3475, doi:10.1175/2011JCLI4208.1.

Sinclair, M. R., 2002: Extratropical transition of Southwest Pacific tropical cyclones. Part I: Climatology and mean structure changes. *Mon. Wea. Rev.*, **130 (3)**, 590–609, doi:10.1175/1520-0493(2002)130⟨0590:ETOSPT⟩2.0.CO;2.

Sousounis, P., and M. Desflots, 2010: Evaluating the impacts of extratropical transitioning on typhoon losses via synoptic case studies. *Twenty-ninth Conference on Hurricanes and Tropical Meteorology*, Tucson, Arizona.

Studholme, J., K. Hodges, and C. Brierley, 2015: Objective determination of the extratropical transition of tropical cyclones in the Northern Hemisphere. *Tellus A*, **67 (0)**, doi:10.3402/tellusa.v67.24474.

Thorncroft, C., and S. C. Jones, 2000: The extratropical transitions of hurricanes Felix and Iris in 1995. *Mon. Wea. Rev.*, **128 (4)**, 947–972, doi:10.1175/1520-0493(2000)128⟨0947:TETOHF⟩2.0.CO;2.

Vimont, D. J., and J. P. Kossin, 2007: The atlantic meridional mode and hurricane activity. *Geophys. Res. Lett.*, **34 (7)**, doi:10.1029/2007GL029683.

Wang, B., and J. C. L. Chan, 2002: How strong ENSO events affect tropical storm activity over the western North Pacific. *J. Climate*, **15 (13)**, 1643–1658, doi:10.1175/1520-0442(2002)015⟨1643:HSEEAT⟩2.0.CO;2.

Wood, K. M., and E. A. Ritchie, 2014: A 40-year climatology of extratropical transition in the eastern North Pacific. *J. Climate*, **27 (15)**, 5999–6015, doi:10.1175/JCLI-D-13-00645.1.

Zarzycki, C. M., D. R. Thatcher, and C. Jablonowski, 2016: Objective tropical cyclone extratropical transition detection in high-resolution reanalysis and climate model data. *Journal of Advances in Modeling Earth Systems*, n/a–n/a, doi:10.1002/2016MS000775.

Zhang, W., G. A. Vecchi, H. Murakami, G. Villarini, and L. Jia, 2016: The Pacific meridional mode and the occurrence of tropical cyclones in the western North Pacific. *J. Climate*, **29 (1)**, 381–398, doi:10.1175/JCLI-D-15-0282.1.

Zhang, W., G. A. Vecchi, G. Villarini, H. Murakami, A. Rosati, X. Yang, L. Jia, and F. Zeng, 2017: Modulation of western North Pacific tropical cyclone activity by the Atlantic Meridional Mode. *Climate Dyn.*, **48 (1)**, 631–647, doi:10.1175/JCLI-D-12-00210.1.

644 Zhu, Y., 2003: *Large-scale Inhomogeneous Thermodynamics – And Application for Atmospheric*
645 *Energetics*. Cambridge International Science Pub.

LIST OF TABLES

681 TABLE 1. Definitions and acronyms of the ocean basins examined in this study, including their sources of
682 best-track datasets, number of storms, and peak seasons (ASO: August-October, JASO: July-October, JAS: July-
683 September, OND: October-December, JFM: January-March, and DJF: December-February). The time period is
684 1979-2015 for all basins.

Basin	**Code**	**Source of best-tracks**	**# Storms**	**Longitudes**	**Peak season**
North Atlantic	NAT	NHC	456	American coast to 30°E	ASO
Western North Pacific	WNP	JMA, JTWC	941, 950	100°E-180°	JASO
Eastern and Central North Pacific	ENP	NHC	610	180° to American coast	JAS
North Indian Ocean	NI	JTWC	179	30°E-100°E	OND
South Indian Ocean	SI	JTWC	334	30°E-90°E	JFM
Australian region	AUS	JTWC	377	90°E-160°E	JFM
South Pacific	SP	JTWC	225	160°E-120°W	JFM

TABLE 2. Summary of ET fractions for the time period 1979-2015, derived in JRA-55 and ERA-Interim. Values are given as percentages and as number of ET storms out of the total number of storms in each basin.

	JRA-55		**ERA-Interim**	
NAT	47.8%	(218/456)	53.7%	(245/456)
WNP (JMA)	46.7%	(439/941)	53.6%	(504/941)
WNP (JTWC)	28.3%	(269/950)	37.5%	(356/950)
ENP	4.8%	(29/610)	23.4%	(143/610)
NI	5.6%	(10/179)	13.4%	(24/179)
SI	11.1%	(37/334)	17.4%	(58/334)
AUS	13.5%	(51/377)	25.2%	(95/377)
SP	28.4%	(64/225)	36.0%	(81/225)

687 TABLE 3. Literature overview of past studies on ET fractions in various basins (no claim to completeness).
688 For comparison, the ET fractions obtained in this study (see Table 2) are added in parentheses (JRA-55/ERA-
689 Interim).

Basin	**Author(s)**	**ET fraction**	**Method / Data**	**Time period (# storms)**
NAT	Hart and Evans (2001)	46% (48%/54%)	NHC best-track labels	1950-1996 (463)
NAT	Studholme et al. (2015)	68% (48%/54%)	CPS and k-means clustering, storms tracked in ECMWF operational analysis	2000-2008 (72)
NAT	Zarzycki et al. (2016)	55% (48%/54%)	CPS, storms tracked in ERA-Interim	1980-2002 (87)
WNP	Klein et al. (2000)	27% (47%/54%)	Satellite imagery, NOGAPS	1994-1998 (112)
WNP	Kitabatake (2011)	49% 40% (47%/54%)	JMA best-track labels CPS, JRA-25	1974-2004 (687)
WNP	Studholme et al. (2015)	65% (47%/54%)	CPS and k-means clustering, storms tracked in ECMWF operational analysis	2000-2008 (111)
ENP	Wood and Ritchie (2014)	9% (5%/23%)	CPS, JRA-55	1971-2012 (631)
ENP	Studholme et al. (2015)	35% (5%/23%)	CPS and k-means clustering, storms tracked in ECMWF operational analysis	2000-2008 (81)
NI	Studholme et al. (2015)	31% (6%/13%)	CPS and k-means clustering, storms tracked in ECMWF operational analysis	2000-2008 (32)
SI	Griffin and Bosart (2014)	44% (11%/17%)	Subjective identification of ET cases in best-track data of Météo-France La Réunion, ERA-Interim	1989-2013 (235)
SP	Sinclair (2002)	32% (28%/36%)	Based on # TCs reaching midlatitudes	1970-1996 (251)

690 TABLE 4. Statistics of the time series of ET fractions: Sample mean and standard deviation (JRA-55 / ERA-
691 Interim), p-value of the slope of the linear regression lines (JRA-55 / ERA-Interim), Pearson correlation co-
692 efficient (R) between the JRA-55 and the ERA-Interim time series, and p-value of that correlation coefficient.
693 Statistically significant values are in bold.

Basin	**mean [%]**	**stdev [%]**	**p-value of slope**	**R**	**p-value of R**
NAT	47.4 / 54.7	17.8 / 16.8	9.60E-01 / 2.92E-01	0.85	**3.49E-11**
WNP	46.9 / 53.6	9.8 / 9.7	1.66E-01 / 3.18E-01	0.90	**5.06E-14**
ENP	4.8 / 24.1	4.7 / 8.3	6.68E-02 / 1.79E-01	-0.11	5.17E-01
NI	6.3 / 15.9	13.0 / 18.2	9.82E-01 / 1.41E-01	0.37	**2.44E-02**
SI	11.3 / 17.7	12.3 / 14.3	**4.91E-03** / 1.83E-01	0.64	**1.74E-05**
AUS	13.6 / 25.4	10.4 / 12.7	2.65E-01 / 7.66E-01	0.50	**1.48E-03**
SP	27.5 / 34.5	23.9 / 21.9	6.72E-02 / 5.93E-01	0.53	**7.79E-04**

TABLE 5. Overview of the storm types at landfall (1979-2015): Based on the CPS parameters calculated in JRA-55 and in ERA-Interim, a storm's type at landfall time is considered tropical (trop), transitioning (trans), or extratropical (extratrop). For comparison, the classification (tropical or extratropical) resulting from the best-track labels is shown as well. If a storm makes multiple landfalls, each individual landfall is counted – thus, the total landfalls exceed the number of landfalling storms. In parentheses, the number of landfalls in each category is given as a percentage of the total landfalls in each basin. Numbers that only refer to the time period 2003-2015 are marked with an asterisk.

			JRA-55			**ERA-Interim**			**Best-Track Labels**	
Basin	Landfalling storms (% of total)	Total landfalls	trop	trans	extra-trop	trop	trans	extra-trop	trop	extra-trop
NAT	205 (45.0%)	347	249 (71.8%)	32 (9.2%)	66 (19.0%)	233 (67.1%)	29 (8.4%)	85 (24.5%)	233 (67.1%)	114 (32.9%)
WNP	542 (57.6%)	941	692 (73.5%)	99 (10.5%)	150 (15.9%)	589 (62.6%)	143 (15.2%)	209 (22.2%)	663 (70.5%)	278 (29.5%)
ENP	85 (13.9%)	107	100 (93.5%)	1 (0.9%)	6 (5.6%)	76 (71.0%)	4 (3.7%)	27 (25.2%)	107 (100.0%)	0 (0.0%)
NI	134 (74.9%)	160	152 (95.0%)	5 (3.1%)	3 (1.9%)	142 (88.8%)	7 (4.4%)	11 (6.9%)	55* (94.8%)	3* (5.2%)
SI	77 (23.1%)	95	95 (100.0%)	0 (0.0%)	0 (0.0%)	94 (98.9%)	1 (1.1%)	0 (0.0%)	30* (85.7%)	5* (14.3%)
AUS	140 (37.1%)	209	200 (95.7%)	4 (1.9%)	5 (2.4%)	190 (90.9%)	6 (2.9%)	13 (6.2%)	65* (91.5%)	6* (8.5%)
SP	31 (13.8%)	32	24 (75.0%)	4 (12.5%)	4 (12.5%)	22 (68.8%)	6 (18.8%)	4 (12.5%)	3* (60.0%)	2* (40.0%)

TABLE 6. Statistics of transition periods: number of ET events (1979-2015), sample mean and standard deviation of the transition periods in each basin, for the JRA-55 and the ERA-Interim ET classifications. Also shown is the p-value of a two-sided t-test on the sample means of JRA-55 and ERA-Interim, with statistically significant values in bold.

	JRA-55			**ERA-Interim**			
	n_ET	mean [h]	stdev [h]	n_ET	mean [h]	stdev [h]	p-value
NAT	218	38	62	245	35	60	5.23E-01
WNP	439	32	46	504	56	71	**1.64E-09**
ENP	29	9	15	143	55	62	**5.53E-13**
NI	10	24	35	24	33	46	8.83E-01
SI	37	28	40	58	32	42	4.87E-01
AUS	51	25	36	95	55	86	**4.97E-02**
SP	64	27	40	81	34	58	2.42E-01

TABLE 7. Linear correlations between time series of the Nino3.4, AMM, and PMM indices and the annual ET fraction (based on the JRA-55 classification): Pearson correlation coefficients (R) and their p-values. Statistically significant values are in bold.

	Nino3.4		**AMM**		**PMM**	
	R	p-value	R	p-value	R	p-value
NAT	0.123	4.69E-01	-0.024	8.89E-01	-0.240	1.53E-01
WNP	0.272	1.03E-01	-0.057	7.40E-01	0.200	2.36E-01
ENP	0.202	2.31E-01	-0.097	5.69E-01	-0.212	2.09E-01
NI	-0.088	6.05E-01	0.092	5.87E-01	0.181	2.84E-01
SI	-0.025	8.83E-01	0.144	3.96E-01	-0.047	7.84E-01
AUS	-0.209	2.14E-01	0.404	**1.31E-02**	-0.134	4.28E-01
SP	-0.277	9.67E-02	0.435	**7.16E-03**	-0.101	5.52E-01

LIST OF FIGURES

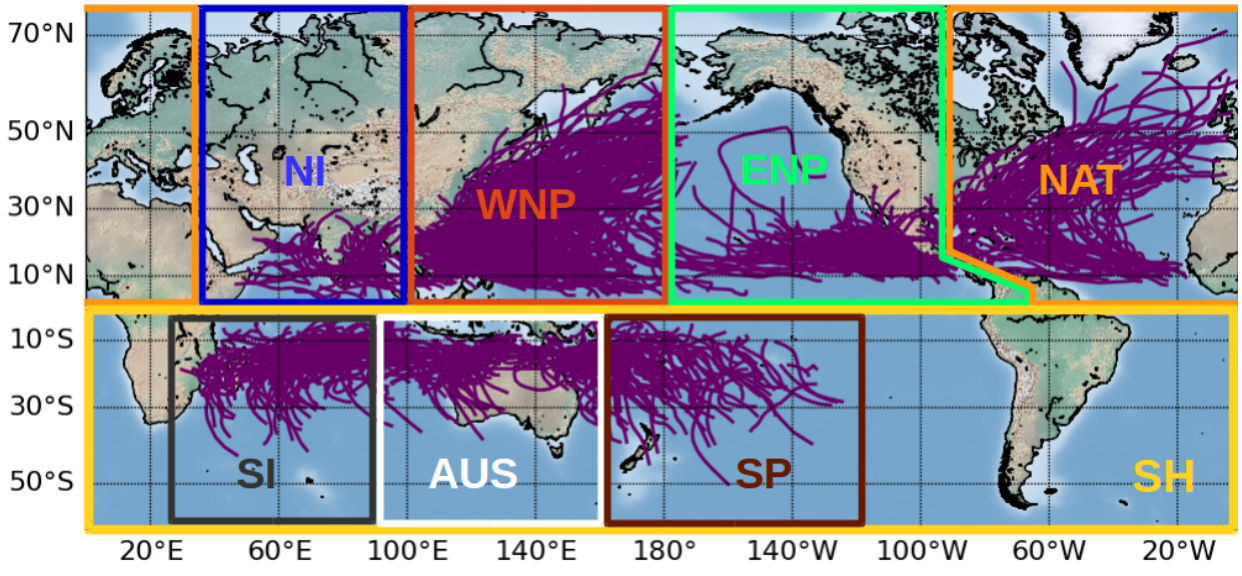

FIG. 1. Global best-tracks of TCs from 1990 to 2000, and the boundaries of the domains examined in this study.

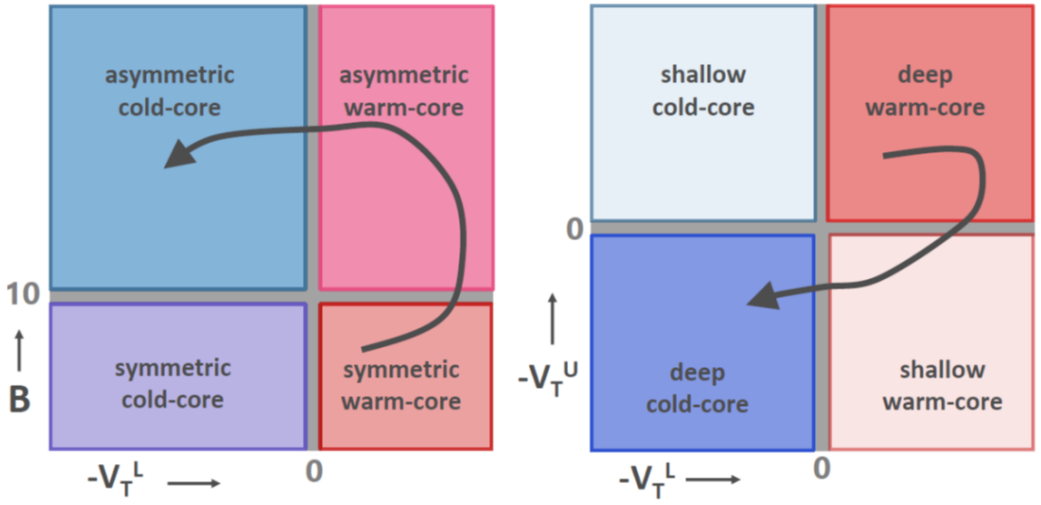

766 FIG. 2. Two cross sections (left: B vs. $-V_T^L$; right: $-V_T^U$ vs. $-V_T^L$) of the CPS proposed by Hart (2003). The
767 arrows trace out idealized paths of a storm undergoing ET, illustrating how its physical structure changes (left)
768 from symmetric warm-core to asymmetric cold-core, and (right) from deep warm-core to deep cold-core.

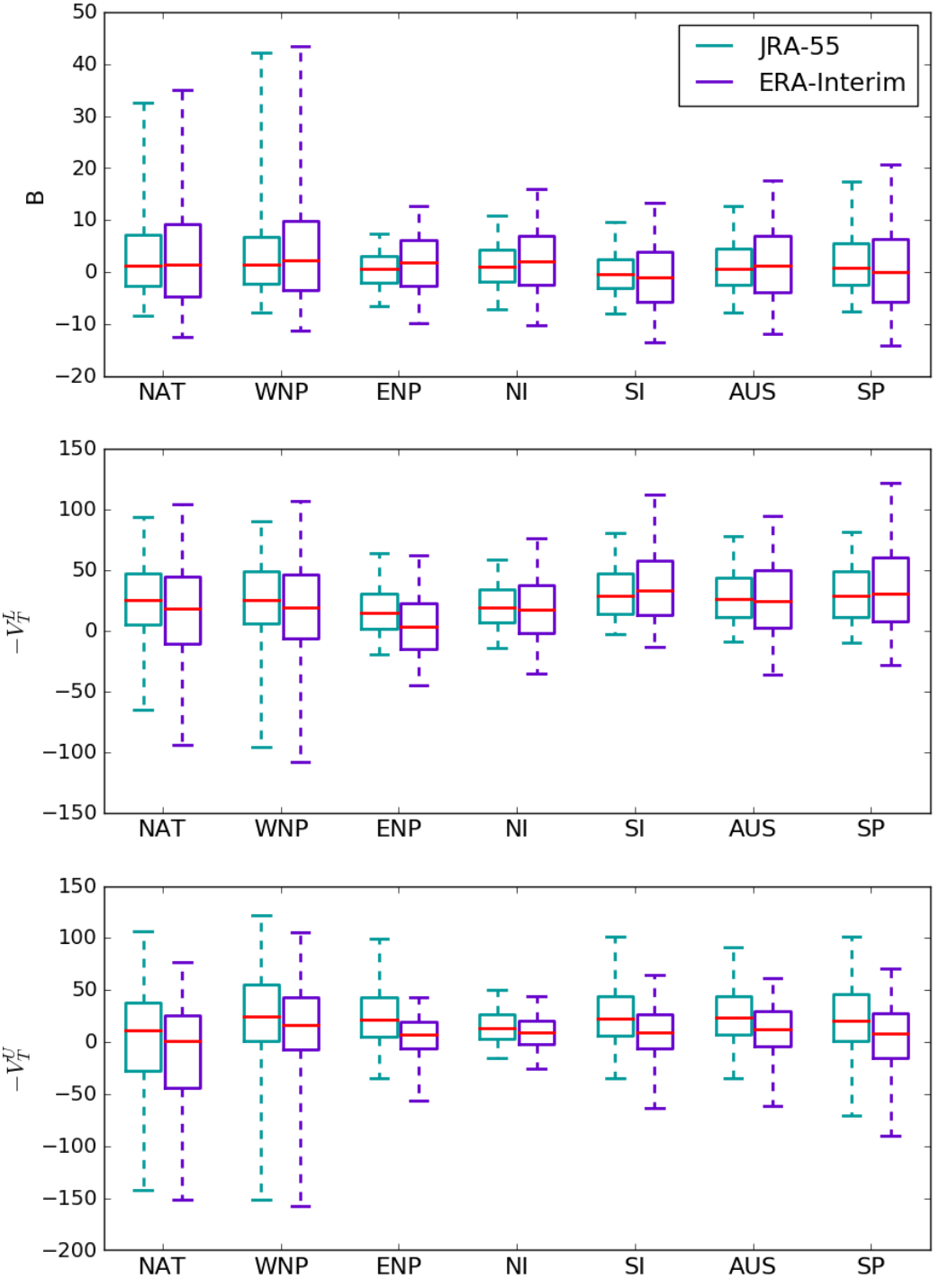

FIG. 3. Box and whisker plots for the CPS parameters, calculated in JRA-55 and ERA-Interim. The box extends from the lower to the upper quartile, with a red line at the median, and the whiskers extend from the 5th to the 95th percentile.

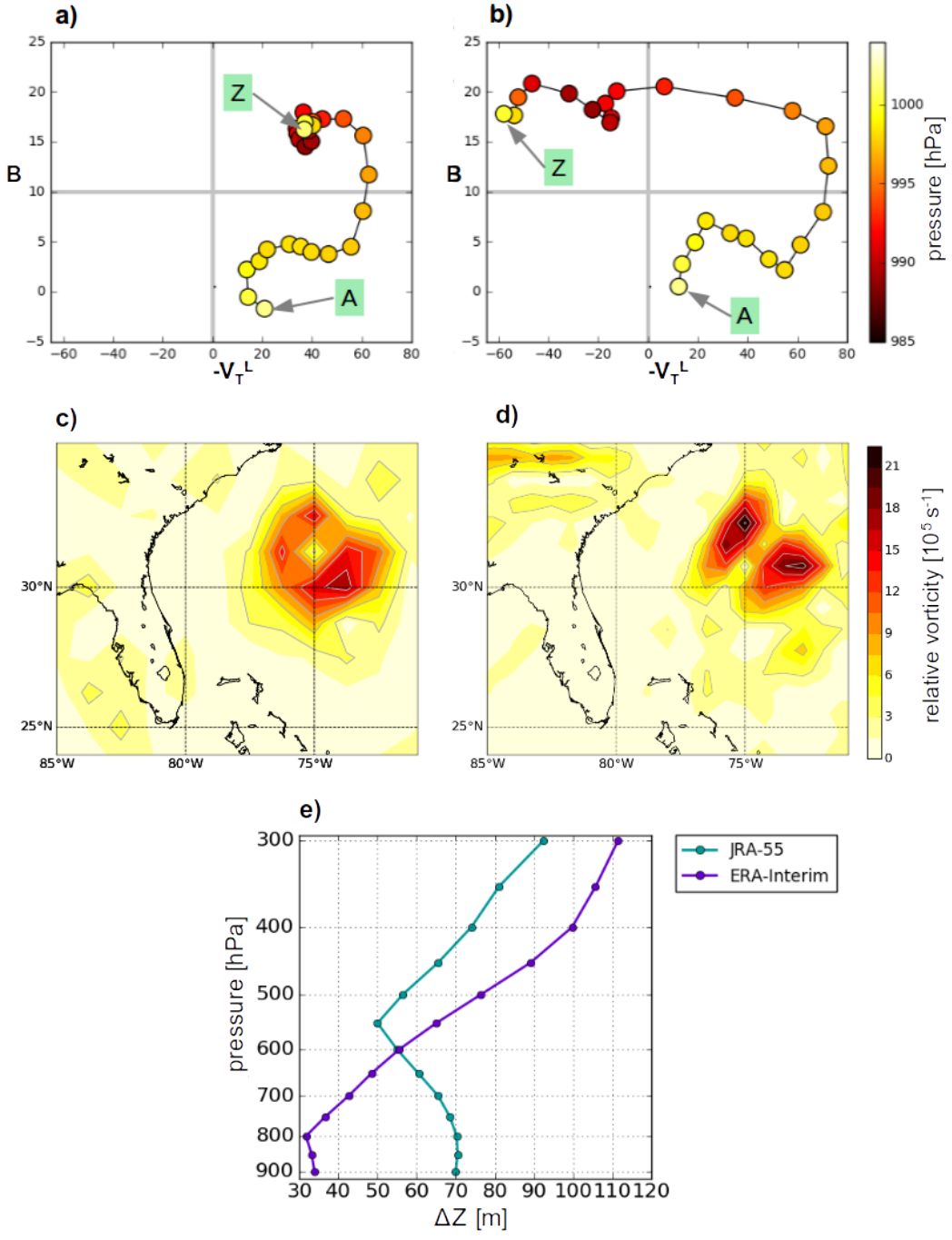

FIG. 4. Trajectory of tropical storm Earl (1992) in a B vs. $-V_T^L$ cross section of the CPS. The CPS parameters in a) were calculated in JRA-55, while b) is based on ERA-Interim data. A and Z mark the beginning and end of the track, respectively. The magnitude of relative vorticity at 850 hPa in (c) JRA-55 and (d) ERA-Interim is shown on 06 UTC 3 October 1992, in units of 10^5 s^{-1}. In (e), ΔZ is the difference between the maximum and minimum geopotential height within a 500 km radius about the reanalysis-specific storm center, taken at the same date and time.

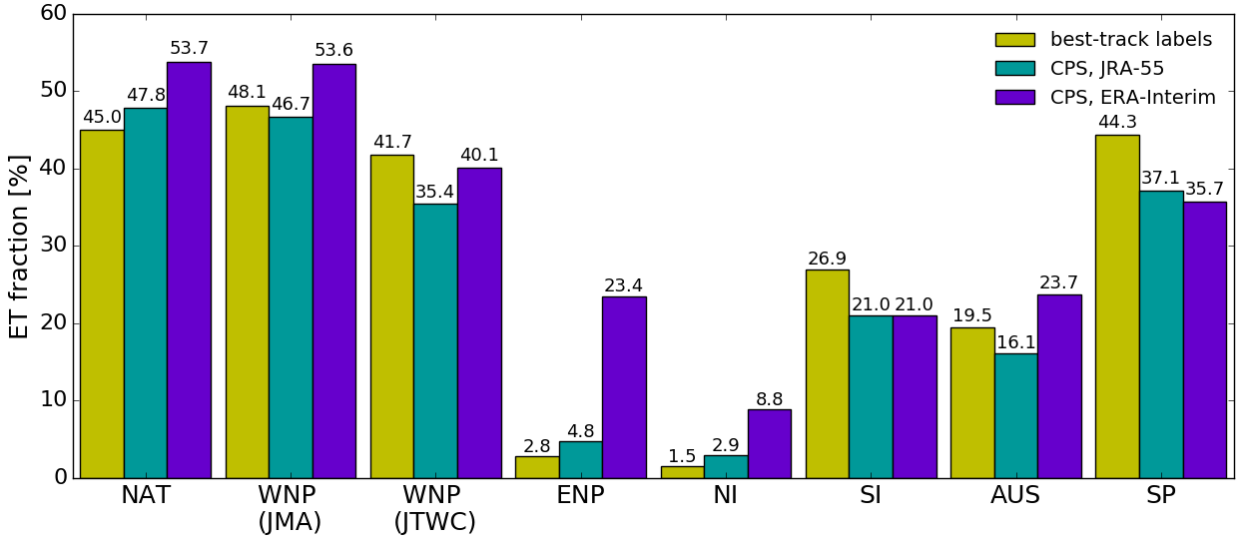

778 FIG. 5. Global ET fractions computed from the objective detection of ET in CPS (in JRA-55 and ERA-
779 Interim) as well as from the storm type labels assigned in the best-track datasets. In the NAT, the WNP (JMA)
780 and the ENP, the fractions are based on the period 1979-2015, while the fractions for the WNP (JTWC), NI, SI,
781 AUS, and the SP refer to the period 2003-2015. The results for the WNP are shown for the best-track archives
782 of JMA as well as JTWC.

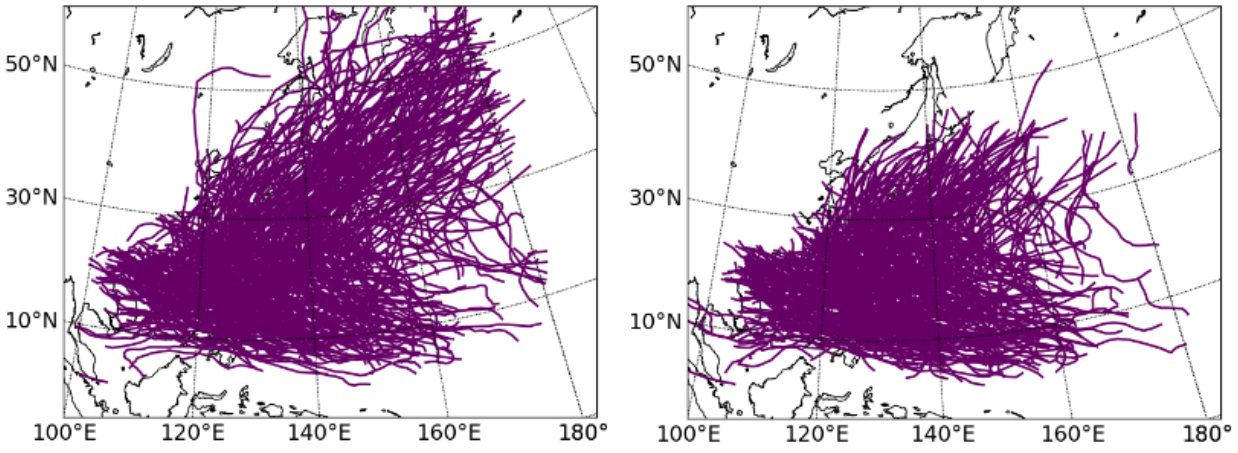

FIG. 6. TC tracks in the WNP (2000-2015), from the JMA (left) and the JTWC (right) best-track archives.

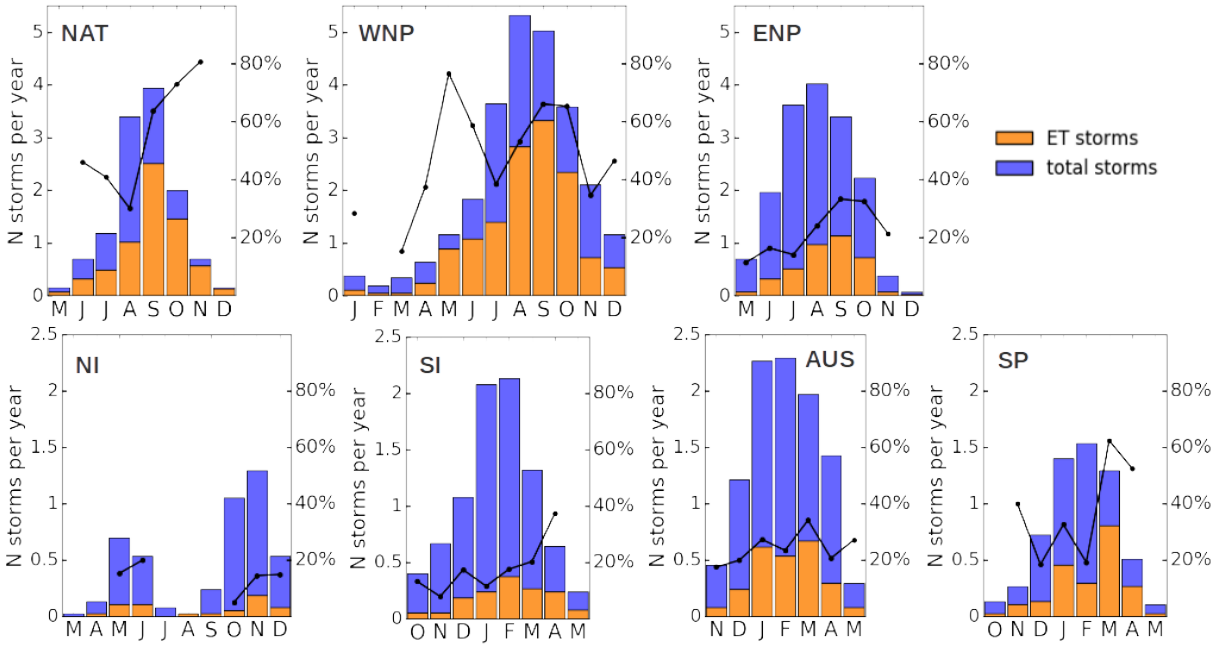

783 FIG. 7. Seasonal cycles of ET in terms of the average annual number of storms in each month (blue: total
784 storms; orange: ET storms, as defined by the JRA-55 classification) for the time period 1979-2015. The black
785 line refers to the percentage axis and shows the corresponding ET fraction, which is only calculated if a minimum
786 of 10 storms (including non-ET storms) occurred in a given month over the whole time period.

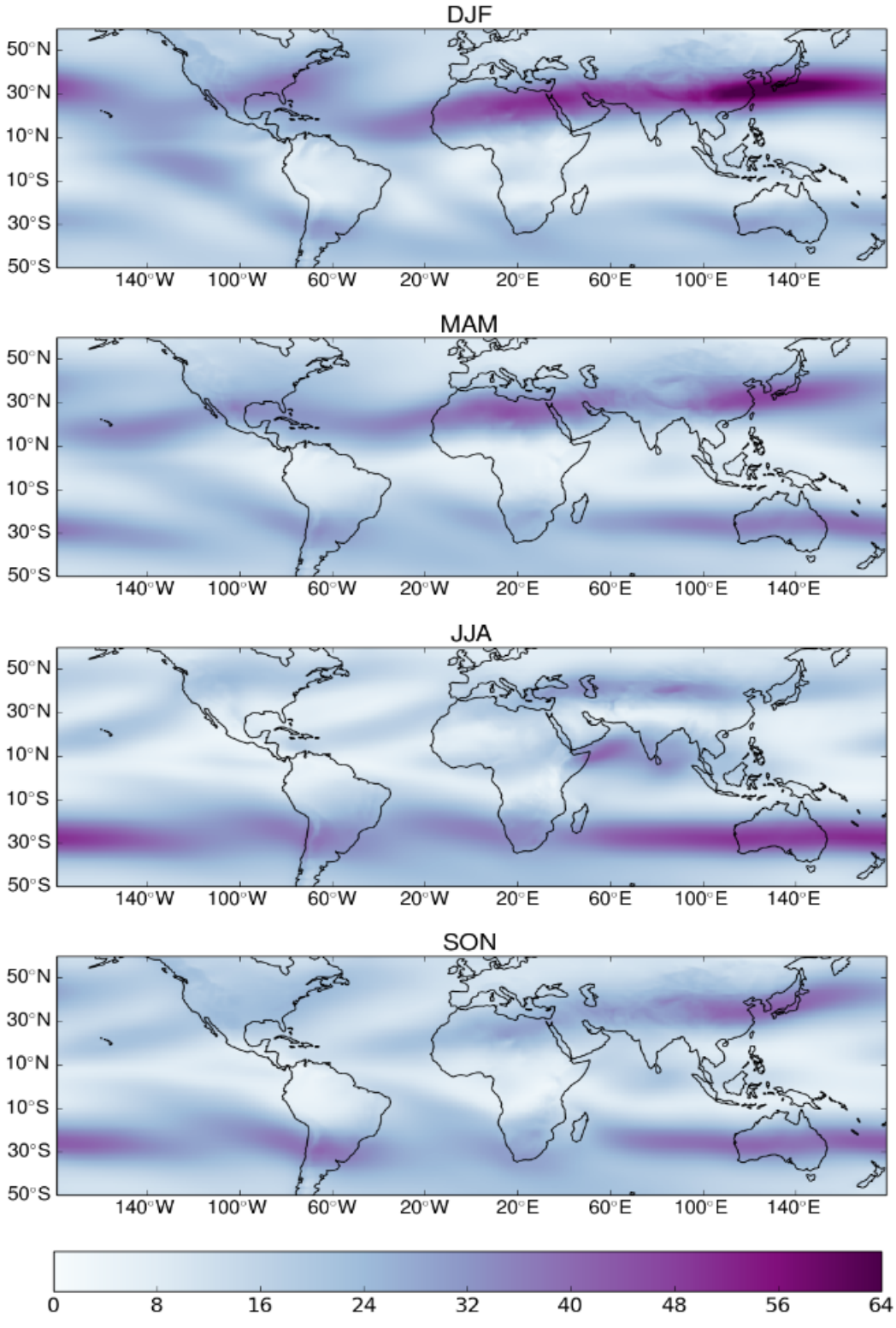

FIG. 8. Seasonal climatologies (1979-2015) of vertical wind shear (units: ms^{-1}), calculated as the magnitude of the vector difference between the wind at 200 hPa and 850 hPa (DJF: December-February, MAM: March-April, JJA: June-August, and SON: September-November). The data source is ERA-Interim.

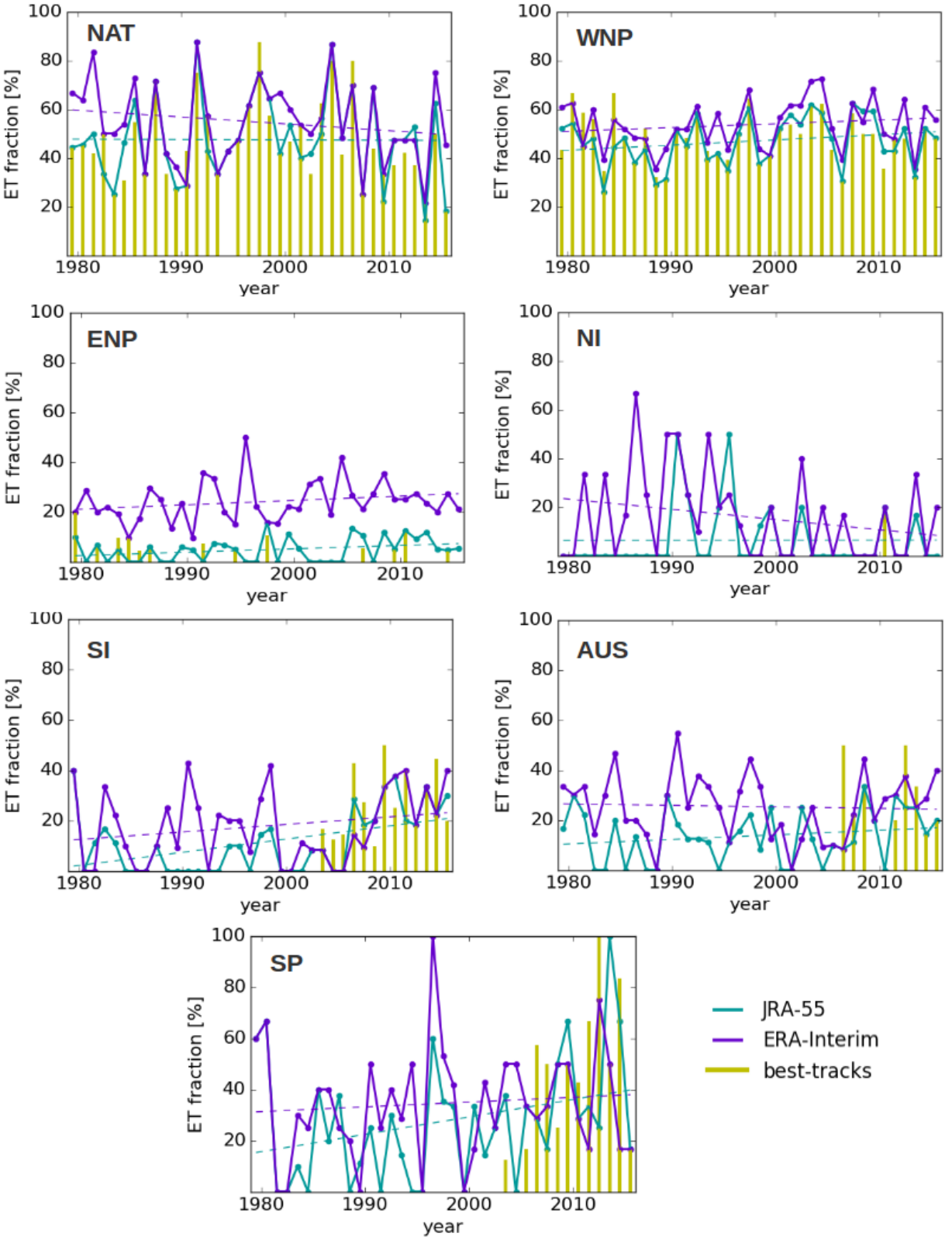

790 FIG. 9. Time series of annual ET fractions from 1979 to 2015, for JRA-55 and ERA-Interim, with dashed
791 lines representing the linear regression best fits to the time series. The vertical bars show the ET fractions derived
792 from the best-track labels.

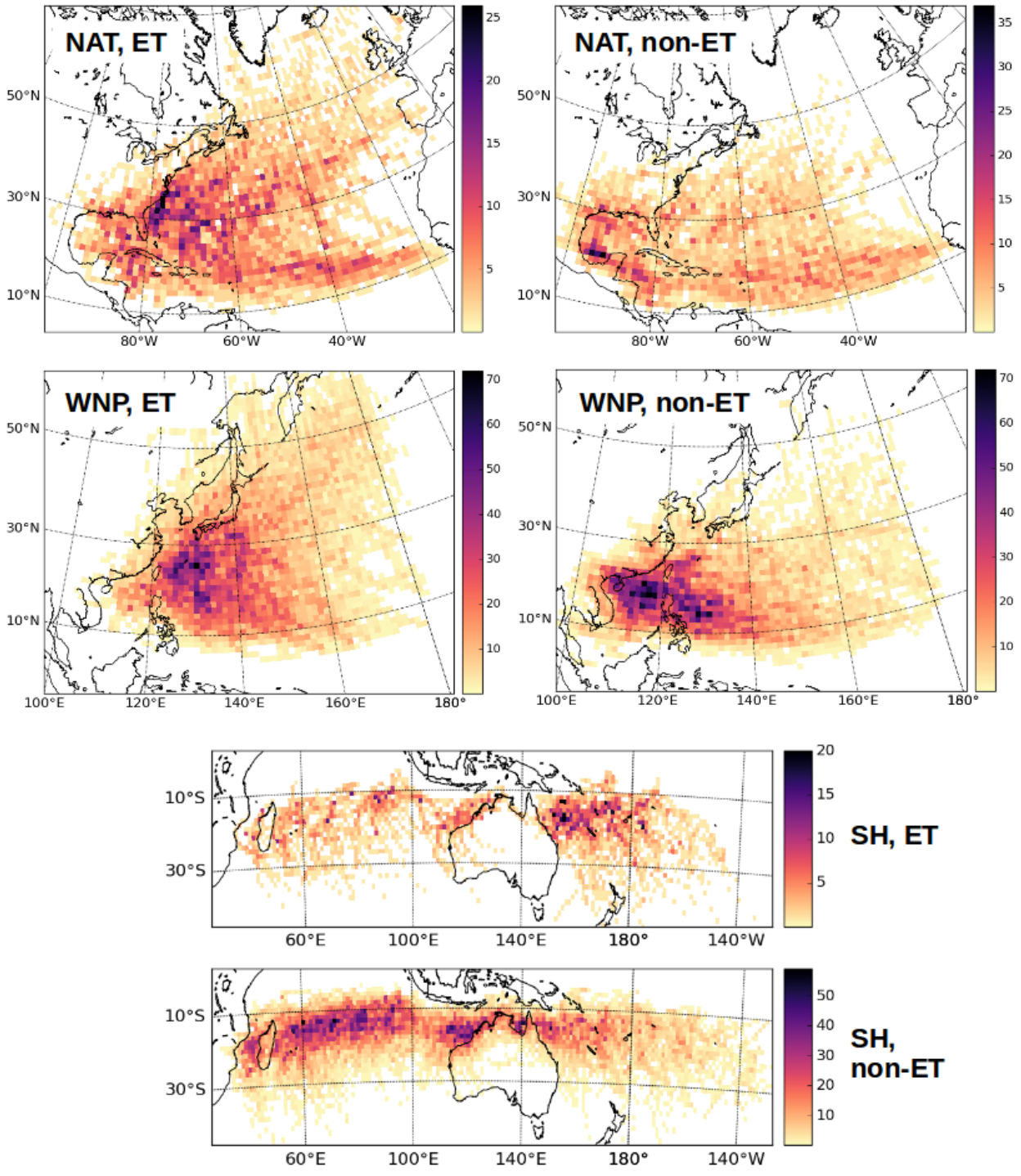

793 FIG. 10. Track density of ET storms and non-ET storms (as defined by the JRA-55 classification) in the NAT,
794 the WNP, and the SH, showing the sum of all best-track data points falling into each $1.25^\circ \times 1.25^\circ$ grid box over
795 the time period 1979-2015.

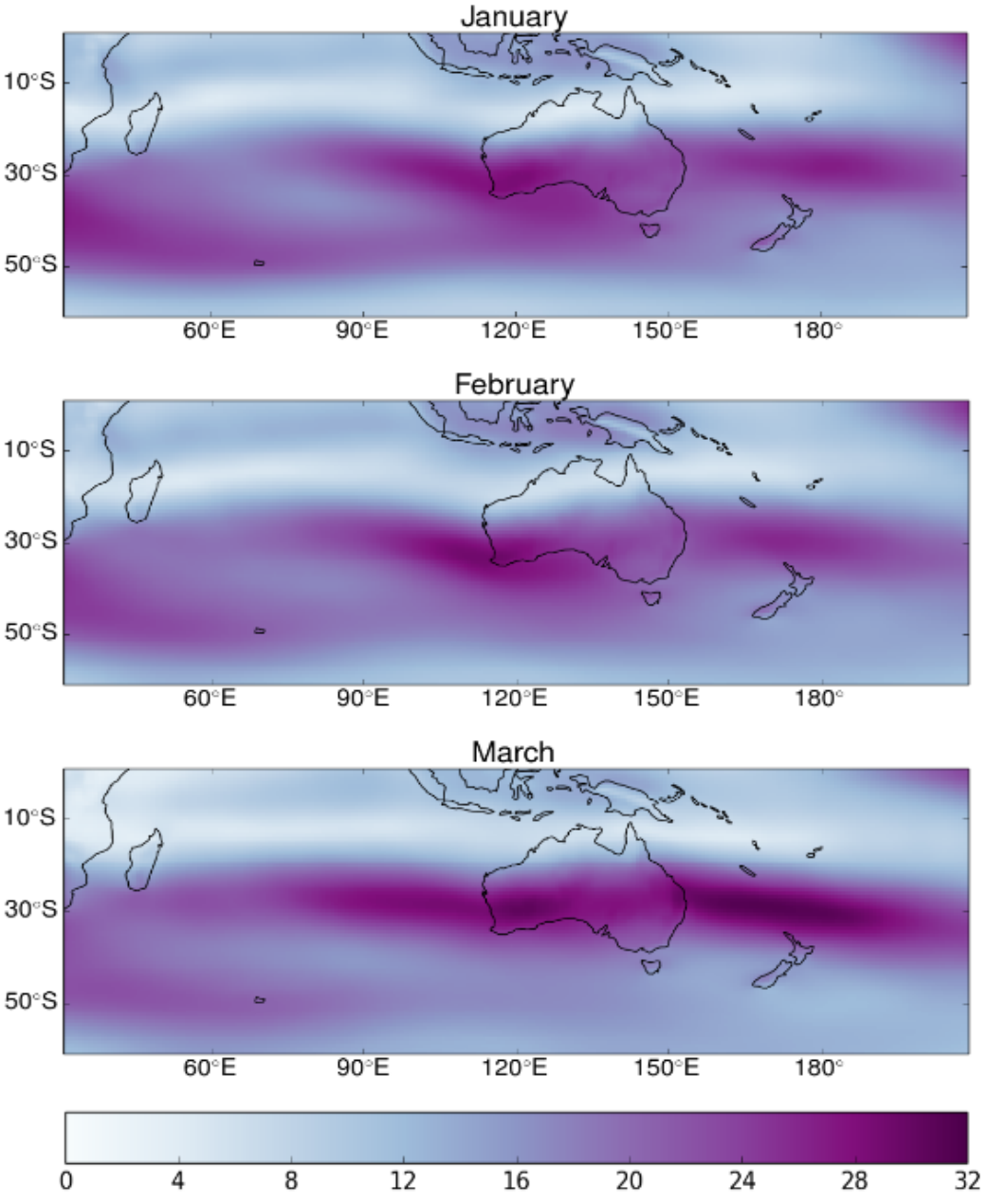

796 FIG. 11. Monthly climatologies (1979-2015) of vertical wind shear (units: ms^{-1}) in the SH basins, for
797 January, February, and March. The vertical wind shear is calculated as the magnitude of the vector difference
798 between the wind at 200 hPa and 850 hPa. The data source is ERA-Interim.

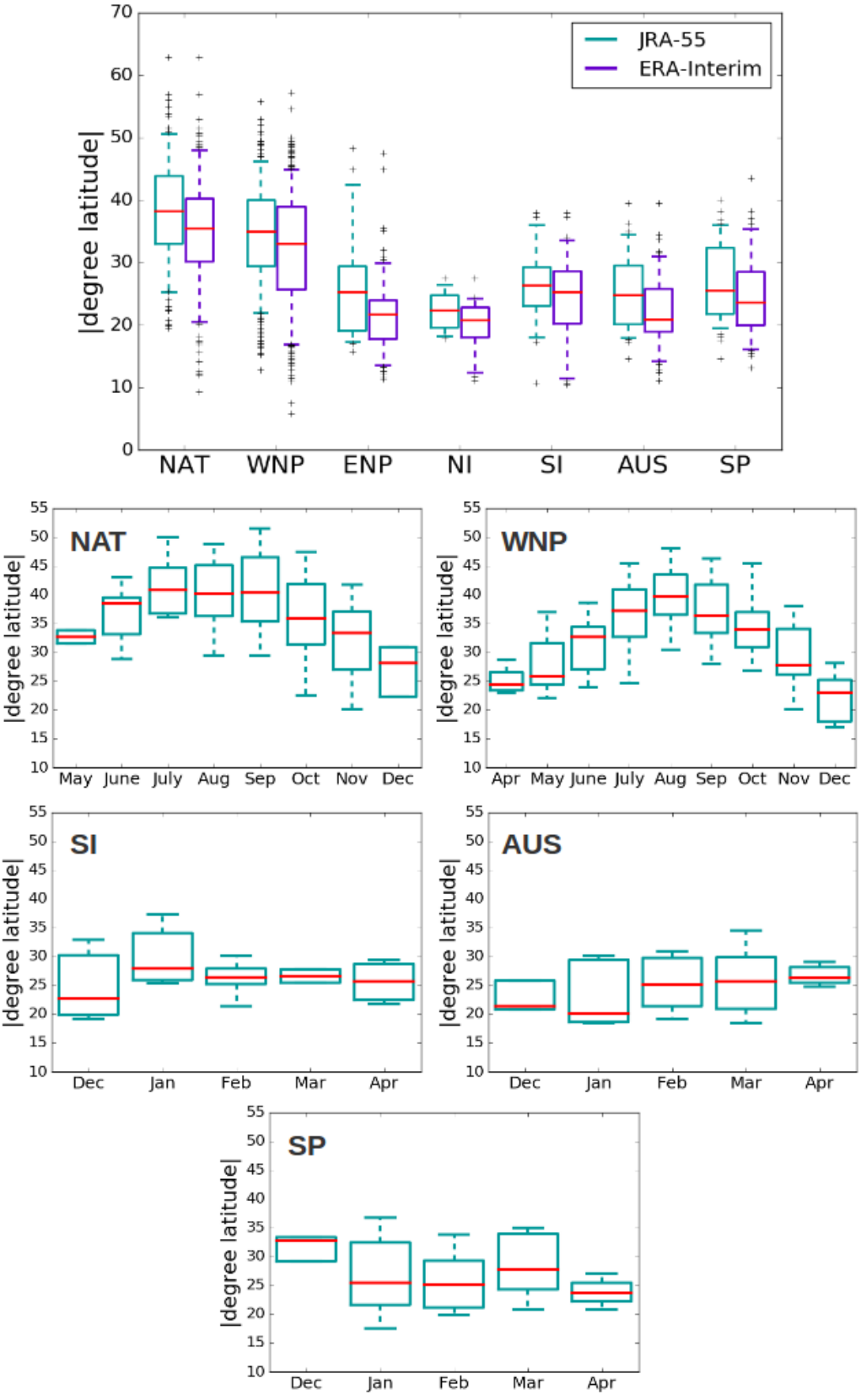
JRA-55
ERA-Interim
|degree latitude|
NAT
WNP
ENP
NI
SI
AUS
SP
May June July Aug Sep Oct Nov Dec
Apr May June July Aug Sep Oct Nov Dec
Dec Jan Feb Mar Apr

FIG. 12. Box plots of the absolute values of the latitudes at which storms complete ET, for all basins and all ETs in 1979-2015 (top; for JRA-55 and ERA-Interim), and decomposition into seasonal cycles for the NAT, WNP, SI, AUS, and the SP (for JRA-55). The box extends from the lower to the upper quartile, with a red line at the median, and the whiskers extend from the 5^{th} to the 95^{th} percentile.The monthly statistics for the ENP and the NI have been excluded due to the scarcity of ET events in those basins.

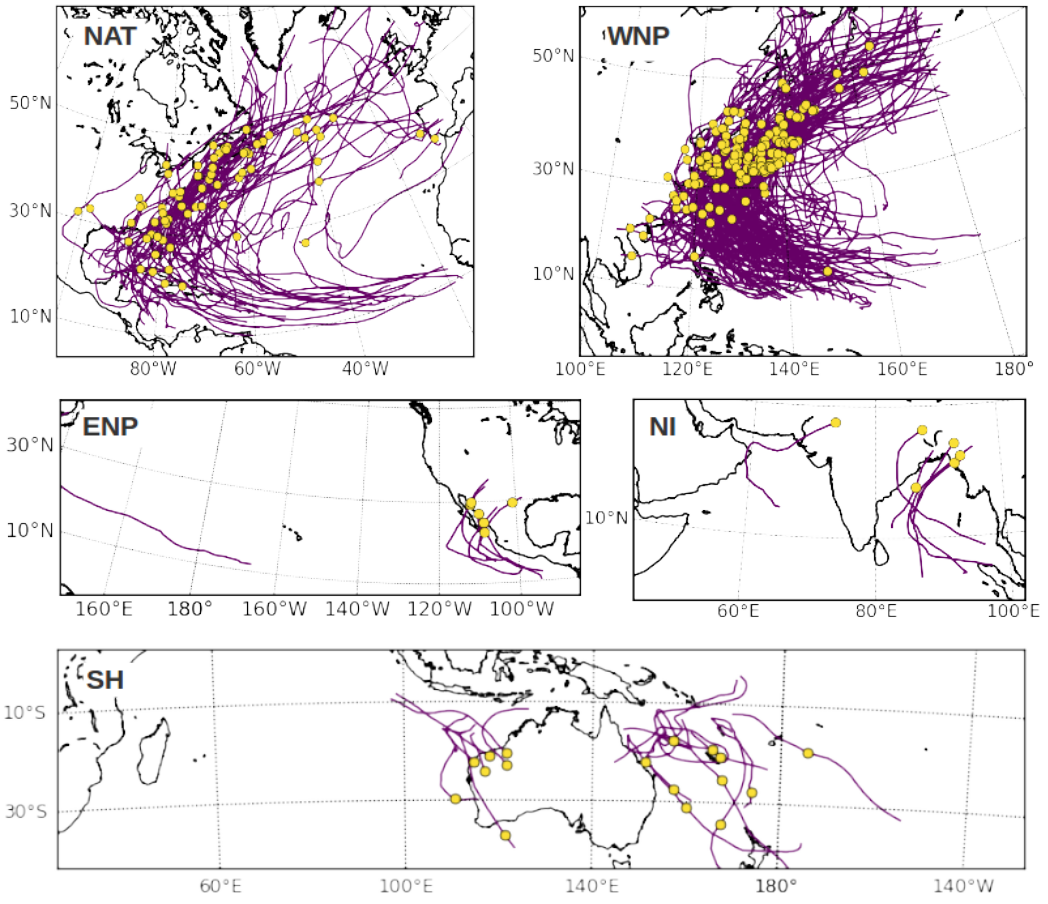

804 FIG. 13. Tracks of storms that make landfall as transitioning or extratropical systems (according to the JRA-55
805 classification), for the time period 1979-2015. The yellow dots mark the locations of ET completion.

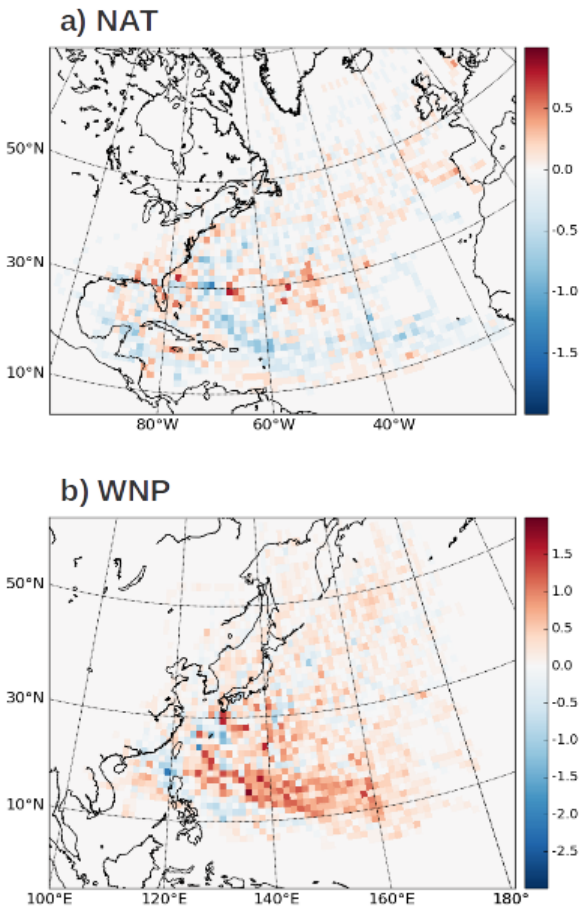

FIG. 14. Difference in the spatial distribution of ET storms (as defined by the JRA-55 classification) between El Niño and La Niña years in (a) the NAT and (b) the WNP: The colors represent the difference between the sum of all best-track data points of ET storms falling into each $1.25^\circ \times 1.25^\circ$ grid box during El Niño years and the corresponding sum of track points during La Niña years. The two sums are normalized by the number of El Niño and La Niña years, respectively.